Molecular Therapy
Original Article

Critical role of TPRN rings in the stereocilia for hearing

Jieyu Qi,[1,2,3,8] Fangzhi Tan,[1,8] Liyan Zhang,[1,8] Yinyi Zhou,[1] Ziyu Zhang,[1] Qiuhan Sun,[1] Nianci Li,[1] Yuan Fang,[1] Xin Chen,[1] Yunhao Wu,[1] Guisheng Zhong,[4,5] and Renjie Chai[1,2,3,6,7]

[1]State Key Laboratory of Digital Medical Engineering, Department of Otolaryngology Head and Neck Surgery, Zhongda Hospital, School of Life Sciences and Technology, School of Medicine, Advanced Institute for Life and Health, Jiangsu Province High-Tech Key Laboratory for Bio-Medical Research, Southeast University, Nanjing 210096, China; [2]Co-Innovation Center of Neuroregeneration, Nantong University, Nantong 226001, China; [3]School of Life Science, Beijing Institute of Technology, Beijing 100081, China; [4]iHuman Institute, ShanghaiTech University, Shanghai 201210, China; [5]School of Life Science and Technology, ShanghaiTech University, Shanghai 201210, China; [6]Department of Otolaryngology Head and Neck Surgery, Sichuan Provincial People's Hospital, University of Electronic Science and Technology of China, Chengdu 610072, China; [7]Southeast University Shenzhen Research Institute, Shenzhen 518063, China

Inner ear hair cells detect sound vibration through the deflection of mechanosensory stereocilia. Cytoplasmic protein TPRN has been shown to localize at the taper region of the stereocilia, and mutations in TPRN cause hereditary hearing loss through an unknown mechanism. Here, using biochemistry and dual stimulated emission depletion microscopy imaging, we show that the TPRN, together with its binding proteins CLIC5 and PTPRQ, forms concentric rings in the taper region of stereocilia. The disruption of TPRN rings, triggered by the competitive inhibition of the interaction of TPRN and CLIC5 or exogenous TPRN overexpression, leads to stereocilia degeneration and severe hearing loss. Most importantly, restoration of the TPRN rings can rescue the damaged auditory function of *Tprn* knockout mice by exogenously expressing TPRN at an appropriate level in HCs via promoter recombinant adeno-associated virus (AAV). In summary, our results reveal highly structured TPRN rings near the taper region of stereocilia that are crucial for stereocilia function and hearing. Also, TPRN ring restoration in stereocilia by AAV-*Tprn* effectively repairs damaged hearing, which lays the foundation for the clinical application of AAV-mediated gene therapy in patients with *TPRN* mutation.

INTRODUCTION

According to the WHO report on hearing in 2020, human sensorineural hearing loss, one of the most common sensory disabilities, affects over 5% of the world's population. About half of all cases of sensorineural hearing loss are due to genetic mutations in hair cells (HCs) and supporting cells, and mutations in over 100 deafness genes have been identified.[1,2] Among these, mutations in stereocilia-associated genes cause severe defects in hair bundles.[3] In the auditory system, highly differentiated sensory HCs sense and convert sound vibrations into electrical signals. Each HC has a hair bundle that consists of three rows of actin-based protrusions called stereocilia that have increasing heights to form a staircase-like appearance. These stereocilia function as the primary mechanosensory detectors and are responsible for converting mechanical force from sound waves into electrical signals. Stereocilia are deflected in response to sound stimulation, resulting in the opening of mechanical transduction channels in the membrane of the stereocilia tips and the subsequent depolarization of HCs. Neurotransmitters are released after cell depolarization, and signal-receiving auditory nerves conduct the associated action potential to the auditory cortex.[4] The stereocilia are formed by skeletal elements consisting of parallel actin bundles and their associated proteins.[5] At the basal ends of the stereocilia, a conical taper connects the stereocilia and the apical surface of HCs,[6] which serves as the pivot point against the mechanical stimuli of sound waves.[7,8]

Pedigree analyses have identified several mutations in proteins concentrated at or near the taper region that are linked to inherited deafness.[9–16] In the taper region, the human deafness-related proteins RADIXIN, TPRN, CLIC5, MYO6, PTPRQ, and GRXCR2 may form a protein complex that appears to be involved in the actin-membrane linkage in the basal taper region of the aging stereocilia.[17–19] The

Received 24 May 2023; accepted 9 November 2023;
https://doi.org/10.1016/j.ymthe.2023.11.011.

[8]These authors contributed equally

Correspondence: Jieyu Qi, State Key Laboratory of Digital Medical Engineering, Department of Otolaryngology Head and Neck Surgery, Zhongda Hospital, School of Life Sciences and Technology, School of Medicine, Advanced Institute for Life and Health, Jiangsu Province High-Tech Key Laboratory for Bio-Medical Research, Southeast University, Nanjing 210096, China.
E-mail: jieyuqi@seu.edu.cn
Correspondence: Fangzhi Tan, State Key Laboratory of Digital Medical Engineering, Department of Otolaryngology Head and Neck Surgery, Zhongda Hospital, School of Life Sciences and Technology, School of Medicine, Advanced Institute for Life and Health, Jiangsu Province High-Tech Key Laboratory for Bio-Medical Research, Southeast University, Nanjing 210096, China.
E-mail: tanfangzhi@163.com
Correspondence: Guisheng Zhong, iHuman Institute, ShanghaiTech University, Shanghai 201210, China.
E-mail: zhongsh@shanghaitech.edu.cn
Correspondence: Renjie Chai, State Key Laboratory of Digital Medical Engineering, Department of Otolaryngology Head and Neck Surgery, Zhongda Hospital, School of Life Sciences and Technology, School of Medicine, Advanced Institute for Life and Health, Jiangsu Province High-Tech Key Laboratory for Bio-Medical Research, Southeast University, Nanjing 210096, China.
E-mail: renjiec@seu.edu.cn

transmembrane protein PTPRQ, which binds MYO6, is required for the formation of the shaft connectors of the hair bundle.[20] PTPRQ-deficient mice show severe fusion and degeneration of stereocilia in HCs and lack the ankle link structures between stereocilia[21] and have abnormal hearing sensitivity,[22] which is similar to what was observed in the previous study in Myo6 knockout mice. Radixin, which plays a role in regulating actin dynamics, is concentrated near the taper region as well[23,24] and anchors the actin cytoskeleton to the plasma membrane and is the only detectable species of ezrin/radixin/moesin in the stereocilia.[25] Loss of RADIXIN in mice causes increased stereocilia deflection, dramatic stereocilia disruption, and reduced hearing sensitivity.[25,26] CLIC5 directly interacts with the N terminus of GRXCR2,[19] and GRXCR2 binds and restricts TPRN to the base of the stereocilia,[17] which are vital for the morphogenesis of stereocilia and auditory perception. The lack of CLIC5 or GRXCR2 causes submembrane TPRN to diffuse along the whole length of the stereocilia and leads to morphological defects in the stereocilia and subsequent hearing impairment.[17,18] However, it has not been clearly described how TPRN is involved in the specific organization and function of the protein complex at the taper region of stereocilia.

Here, we use super-resolution imaging with stimulated emission depletion microscopy (STED) and found that TPRN formed ring-like structures near the basal taper of the stereocilia, and these ring-like structures were shown to be critical for stereocilia maintenance and normal hearing. Disruption of the TPRN rings showed stereocilia disruption, HC loss, and hearing impairment. Moreover, when *Tprn* was exogenously expressed by the adeno-associated virus (AAV) vector in $Tprn^{\Delta/\Delta}$ neonatal mice, a moderate amount of exogenous TPRN via a modified type I hammerhead ribozyme (HHR) or a weaker enhancer promoter CMV173 was capable of restoring TPRN rings and the auditory brain stem responses (auditory brainstem responses [ABRs]). Our findings thus provide a highlighted insight into how TPRN molecules are organized in the taper region, revealing a critical role of TPRN rings in stereocilia maintenance and hearing, and suggest that gene therapy has the potential to prevent hearing loss in humans with *TPRN* mutations.

RESULTS

TPRN forms a ring around the taper region of the stereocilia

To gain insights into the role of TPRN in mouse hearing, we first examined the location of TPRN in the organ of Corti by immunofluorescence. TPRN was distributed in both HCs and supporting cells and gave strong signals in the taper region of the stereocilia in HCs from postnatal day 6 (P6) mice (Figures 1A and 1B), which was consistent with a previous study.[27]

Recent advances in super-resolution fluorescence microscopy have allowed the visualization of molecules with pinpoint accuracy,[28] and STED techniques have been developed that have improved the effective resolution down to less than 25 nm, thus overcoming the diffraction limit of visible light.[29] STED has been successfully used to obtain high spatial resolution of protein distributions in cellular compartments, such as the circumferential ring of spectrin in the cuticular plate of HCs that we observed previously.[30] To obtain higher spatial resolution of TPRN distribution in the stereocilia, especially in the taper region, we used STED imaging to characterize the distribution of TPRN. Under a confocal microscope at 100× magnification, we observed dot-like foci of TPRN in the stereocilia in both outer hair cells (OHCs) and inner hair cells (IHCs) (Figure 1C). STED showed that TPRN formed organized ring-like structures with diameters ranging from 150 to 200 nm outlining the edges of each stereocilium (Figure 1C).

Recently, Zhao et al. used stochastic optical reconstruction microscopy (STORM) microscopy and found that TPRN appeared as dense puncta extending into the core of the stereocilia,[31] which was not consistent with our results. To exclude the influence of non-specific antibody binding, we inserted a hemagglutinin (HA) tag coding sequence at the C terminus of mouse TPRN immediately prior to the stop codon using CRISPR-Cas9 genome editing (Figure 1D). SpCas9 exceeds the packaging limit of a single AAV. An intein-mediated protein trans-splicing facilitated the large gene transfer capacity mediated by AAV, such as SpCas9.[32] Thus, the split-intein-Cas9 system along with a recombination donor was packaged into three AAV vectors and delivered into HCs via the AAV vector Anc80L65[33] (Figure 1E). Genomic PCR was performed 11 days after injection of virus to confirm that the HA tag was inserted into the genome (Figures S1A–S1D) with a relatively low efficiency (Figure S1E). Consistent with the results above, the HA signal showed similar ring-like structures in three dimensions (Figure 1F), which verified the results obtained with the TPRN antibody. Taken together, these results show that TPRN forms cylindrical structures in the taper region of stereocilia.

The taper region is at the basal end of the stereocilium, where parallel actin filaments begin to narrow and terminate in an ordered manner.[6] The actin in the stereocilia is comprised of β-actin and γ-actin.[34] We visualized the correlation between TPRN and actin *in situ* by dual STED imaging in which actin was labeled with phalloidin-conjugated organic dyes. The STED images showed that each TPRN ring surrounded an actin dot (Figure 1G), supporting the observation that TPRN formed a circumferential ring outlining the cross-sectional edge of individual stereocilia. The spatial proximity suggests that TPRN interacts with actin. Liu et al. have shown that TPRN could modulate the actin cytoskeleton and also put some effort into mapping the region of TPRN needed to cause changes in the actin cytoskeleton.[17] Here, we constructed *Tprn*-overexpression plasmids for performing co-immunoprecipitation (coIP) *in vitro* to verify its interaction with β-actin (Figure 1H). Also, rod-like aggregates of actin were obtained in full-length *Tprn* transduced HeLa cells (Figure 1I), which was consistent with previous report.[17] Taken together, TPRN molecules form neat rings and bind actin filaments in the stereocilia, which may stabilize the stereocilia.

TPRN-CLIC5-PTPRQ rings anchor actin filaments beneath the cytomembrane

As a cytoplasmic protein, how the TPRN ring is formed and anchored in the taper region is unknown. According to a previous study,

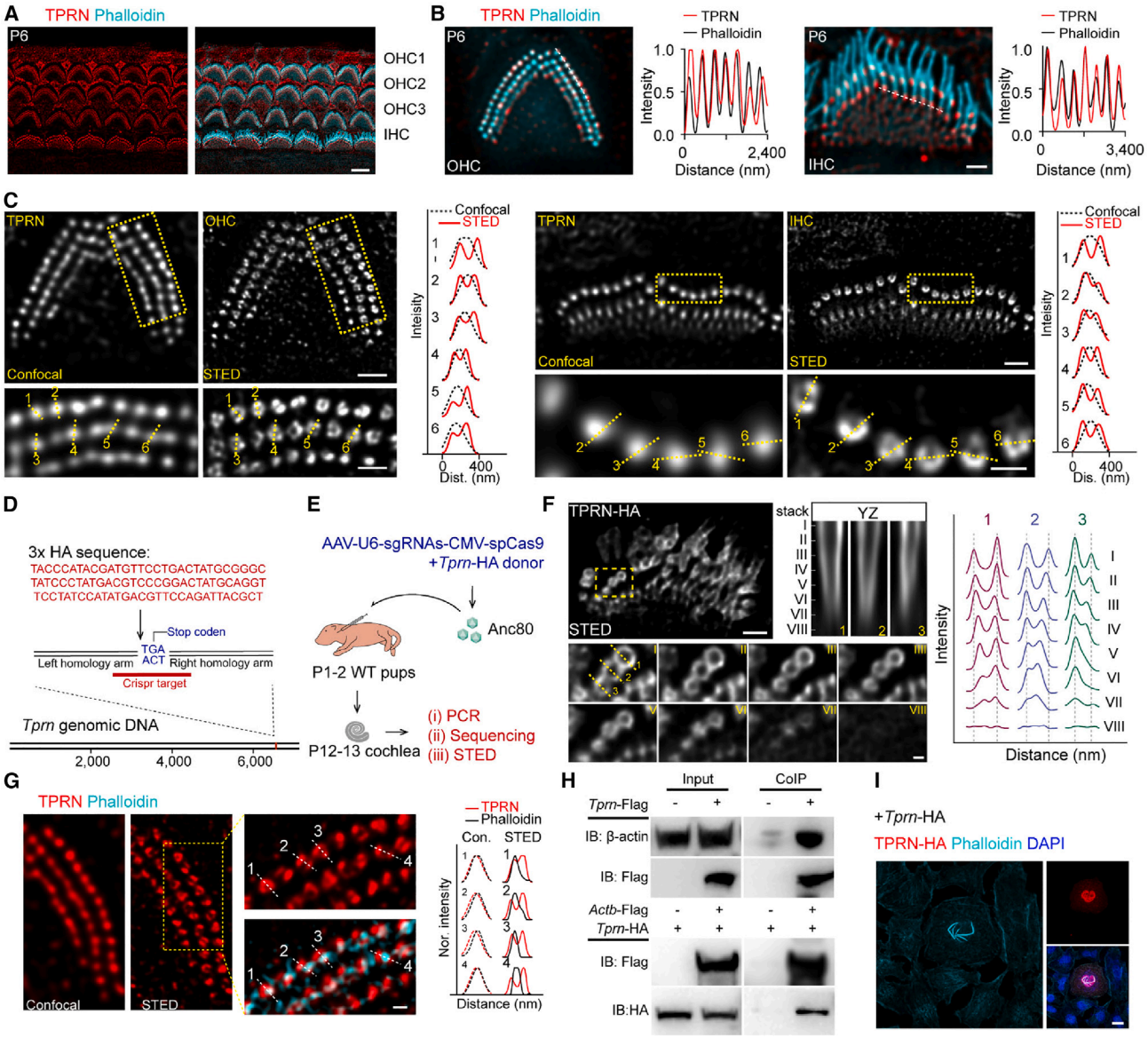

Figure 1. TPRN formed a ring-like structure in the taper region of the stereocilia

(A) Representative confocal images of TPRN (red) and phalloidin (cyan) in the HCs from P6 mice. Scale bar, 5 μm. (B) Dual-color confocal images of TPRN in an OHC or IHC from (A). Intensity profiles corresponding to the dashed lines are shown. Scale bar, 1 μm. (C) Conventional confocal and STED images of TPRN in a mouse OHC and IHC, respectively, with magnification of the yellow boxed regions shown below. Intensity profiles corresponding to the dashed lines (1–6) are shown at the bottom. Scale bars, 1 μm and 500 nm (in the OHC) and 1 μm and 400 nm (in the IHC). (D) Strategy of HA insertion at the end of the *Tprn* coding sequence via AAV and CRISPR-Cas9-mediated homology-directed repair (HDR) in HCs. (E) Depiction of the experimental paradigm for *Tprn*-HA knockin (KI) in mouse cochleae with Anc80L65. The cochleae were collected at P12-13 for further PCR, genomic sequencing, and STED imaging. (F) Conventional STED images of TPRN-HA in an AAV-infected IHC. The HA sequence was inserted at the end of the *Tprn* coding sequence via AAV and CRISPR-Cas9-mediated HDR in IHCs, with a dose of 9×10^{10} GCs in the left ear. Representative serial optical sections (interval = 0.319 μm) of STED images along the z axis magnified from the yellow boxed regions are shown. The rings are numerically labeled, and intensity profiles corresponding to the dashed lines (1–3) are shown. Scale bars, 1 μm and 250 nm. (G) Conventional confocal and STED images of TPRN (red) and phalloidin (cyan) in mouse OHCs at P14. Intensity profiles corresponding to the dashed lines (1–4) are shown beneath. Scale bar, 200 nm. (H) coIP between TPRN and actin. Mouse N2A cells were transfected with the FLAG, *Tprn*-FLAG, *Tprn*-HA, or *Actb*-FLAG constructs. Immunoprecipitations were carried out with FLAG antibodies followed by western blotting to detect co-expressed proteins by using β-actin or HA antibodies. The image is representative of three independent experiments. (I) HeLa cells were transfected with the TPRN-HA construct. TPRN-HA (red), phalloidin (cyan), and DAPI (blue) were stained and imaged after 2 days of transfection. DAPI indicates the nucleus. Scale bar, 20 μm.

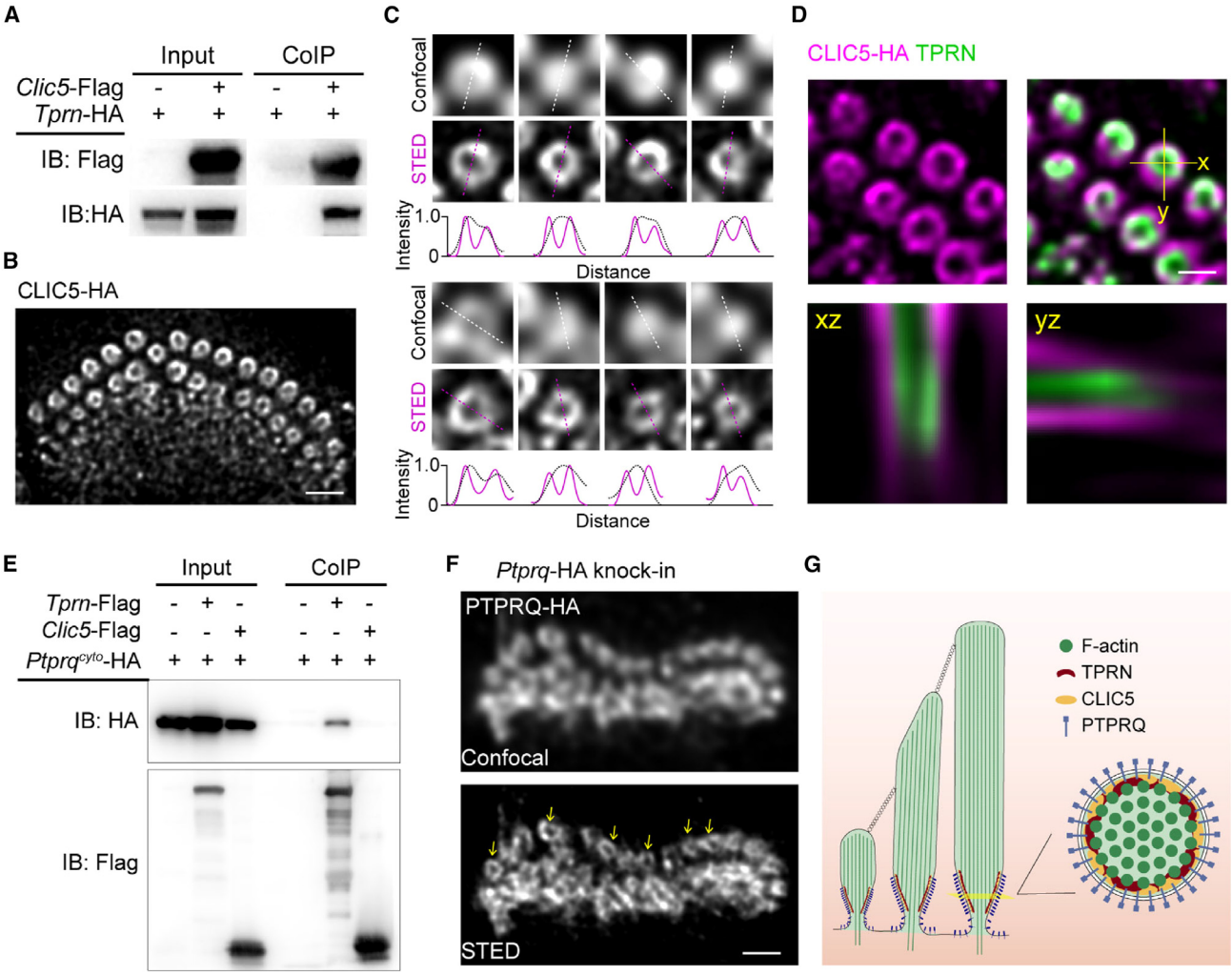

Figure 2. TPRN-CLIC5-PTPRQ formed ring-like complexes in the taper region of stereocilia

(A) HEK293T cells were co-transfected with the FLAG, *Tprn*-FLAG, or *Clic5*-HA constructs. Immunoprecipitations were carried out with FLAG antibodies followed by western blotting to detect co-expressed proteins by using HA antibody. Representative data from three independent experiments. (B) Representative STED image of CLIC5-HA in an IHC at P17 from an Anc80L65-*Clic5*-HA-infected cochlea. Scale bar, 1 μm. (C) Magnified regions in (B) indicated by the arrows. Intensity profiles corresponding to the dashed lines are shown. (D) Representative dual-STED images of CLIC5-HA (magenta) and TPRN (green) in an IHC at P17 from Anc80L65-*Clic5*-HA-infected cochleae at a dose of 4.5×10^{10} GCs at day 17 after surgery at P3. Three-dimensional dual-STED images of the xz and yz axes are shown. Scale bar, 400 nm. (E) HEK293T cells were transfected with the FLAG, *Tprn*-FLAG, *Clic5*-FLAG, or *Ptprq*^{Cyto}-HA construct. Immunoprecipitations were carried out with FLAG antibodies, followed by western blotting to detect co-expressed proteins by using FLAG or HA antibodies. The images are representative of three independent experiments. (F) Conventional confocal and STED images of PTPRQ-HA in an AAV-infected IHC. The HA sequence was inserted at the end of the *Ptprq* coding sequence via AAV and CRISPR-Cas9-mediated HDR in IHCs with a dose of 9×10^{10} GCs in the left ear. Scale bar, 1 μm. (G) Model of the ring-like complex localization pattern in hair cells. In this model, TPRN molecules bind to cytoplasmic CLIC5 and the transmembrane PTPRQ to form polymeric and concentric rings around the actin filaments in the taper region of the stereocilia.

CLIC5, which stabilizes membrane-actin filament linkages at the taper region of stereocilia, interacts directly with TPRN.[35] We confirmed this observation in our coIP experiments (Figure 2A). To visualize their correlation *in situ* we packaged a *Clic5*-HA expression cassette into the AAV vector and delivered it into the cochlea via round window membrane (RWM) injection at P3. Cochleae were harvested at P17 and immunostained with HA and TPRN antibodies together. The CLIC5-HA puncta in the confocal imaging also presented similar ring-like structures in the STED images (Figures 2B and 2C). In addition, CLIC5 showed concentric rings with TPRN, and the three-dimensional STED imaging confirmed this observation (Figure 2D), indicating that the proper localization of TPRN and the formation of the ring-like structure may require CLIC5. As cytoplasmic proteins, the TPRN-CLIC5 complex might need to be anchored to the cell membrane in order to hold the actin filaments in place. PTPRQ is a membrane protein in the taper region,[36,37] and we found that TPRN, not CLIC5, interacted with the C terminus of PTPRQ (Figure 2E). To visualize the structure of PTPRQ, we used

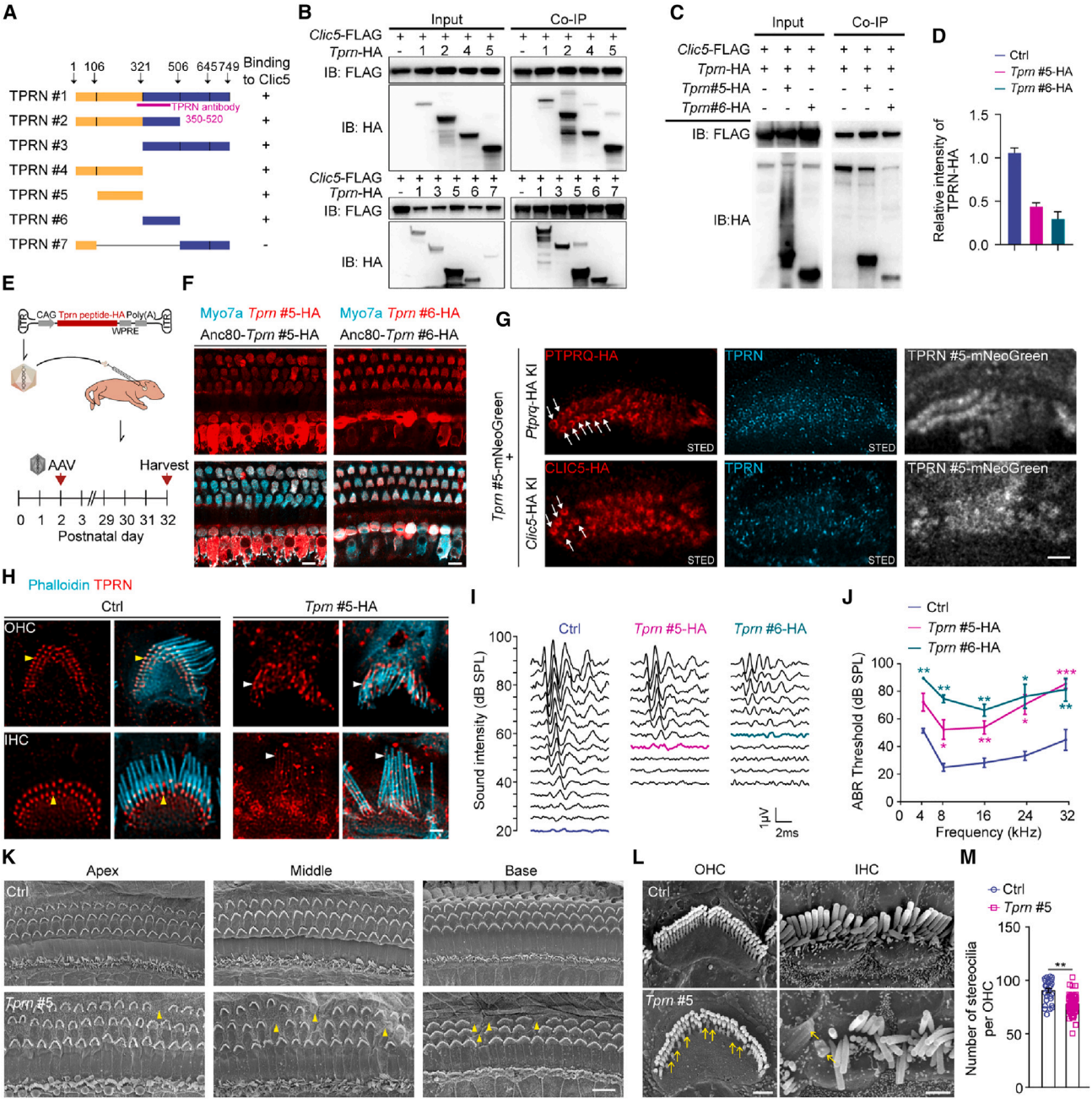

Figure 3. *In vivo* disruption of the interaction between TPRN and CLIC5 resulted in impaired hearing and disrupted sensory epithelia

(A) Diagram of the TPRN fragment constructs used to identify the binding domain with CLIC5. Binding regions are shown by the symbol "+." (B) HEK293T cells were co-transfected with the TPRN fragment constructs and *Clic5*-FLAG constructs. Immunoprecipitations were carried out with FLAG antibodies followed by western blotting to detect co-expressed proteins by using HA antibody. The images are representative of three independent experiments. (C) TPRN fragments no. 5 and no. 6 competitively weakened the interaction between TPRN and CLIC5. HEK293T cells were co-transfected with the TPRN fragments (no. 5 or no. 6) and *Clic5*-FLAG constructs. Immunoprecipitations were carried out with FLAG antibodies followed by western blotting to detect co-expressed proteins by using HA antibody. The images are representative of two independent experiments. (D) Relative signal intensity of immunoprecipitated TPRN-HA in (C). (E) Depiction of the experimental paradigm for the competitive inhibition with TPRN peptide via Anc80L65. All mice were injected with corresponding virus at a dose of 5.25×10^9 or 7.5×10^9 GCs in the left ear. ABR tests were performed and cochleae were collected for further morphology analyses about 4 weeks after injection. (F) Representative confocal images of the cochlea injected with Anc80L65-*Tprn* no. 5-HA or Anc80L65-*Tprn* no. 6-HA. Cyan, Myo7a; red, HA. Scale bar, 10 μm. (G) Representative STED images of PTPRQ-HA and CLIC5-HA in HCs from Anc80L65-*Tprn* no. 5-mNeoGreen-injected cochlea. HA was inserted at the end of the *Ptprq* or *Clic5* coding sequence via AAV and CRISPR-Cas9-mediated homology directed repair. Arrows indicate the rings. Scale bar, 1 μm.

(legend continued on next page)

Cas9-mediated homologous recombination to insert an HA tag onto the end of the *Ptprq* gene coding region and imaged PTPRQ-HA by STED microscopy. PTPRQ showed similar ring structures in cochlear HCs (Figure 2F), thus these results indicate that TPRN, CLIC5, and PTPRQ might form a ring-like cluster complex in the taper region (Figure 2G).

Disruption of TPRN rings leads to severe stereocilia disorders and deafness

We next sought to determine the potential role of the TPRN rings in normal hearing. We first generated several TPRN truncations fused to an HA tag (Figure 3A) to map the protein domains that are critical for the TPRN-CLIC5 interaction. Fragments no. 5 and no. 6 containing amino acids 106–506 in TPRN ($TPRN^{106\text{-}321}$ and $TPRN^{321\text{-}506}$) both had strong affinity for CLIC5 (Figure 3B). Consistent with this, overexpression of $TPRN^{106\text{-}321}$ or $TPRN^{321\text{-}506}$ could competitively inhibit the binding of full-length exogenous TPRN to CLIC5 (Figures 3C and 3D). We next packaged $TPRN^{106\text{-}321}$ or $TPRN^{321\text{-}506}$ with a 3× HA tag into Anc80L65 (transduced HCs with near 100% efficiency[33]), and delivered them into the cochleae of P2 mouse pups. Successful delivery into the HCs was verified by HA and Myo7a (HCs marker) immunostaining (Figures 3E and 3F). Using the similar knockin strategy shown in Figure 1D, the HA tag was inserted at the end of the *Ptprq* or *Clic5* coding sequence via Anc80L65 and CRISPR-Cas9-mediated homology-directed repair, and AAV-$TPRN^{106\text{-}321}$-mNeonGreen was delivered simultaneously. We utilized HA and TPRN antibodies for STED imaging. $TPRN^{106\text{-}321}$ was successfully expressed in the stereocilia (Figure 3G), and the dual-color imaging showed that TPRN rings were no longer localized to the taper region in the HCs transduced by $TPRN^{106\text{-}321}$, while there was no effect on the CLIC5 and PTPRQ rings (Figure 3G). An antibody against amino acids 350–520 was used to detect endogenous TPRN, and the imaging results showed that endogenous TPRN was dispersed along the entire shaft of the stereocilium instead of concentrating in the taper region (Figure 3H), indicating that the truncated protein is competitively expressed in the taper of the stereocilia. Furthermore, the expression of TPRN truncations led to a significant increase in hearing thresholds (Figures 3I and 3J). Next, we used a scanning electron microscope (SEM) to image the stereocilia after $TPRN^{106\text{-}321}$ injection and found that disruption of the TPRN-CLIC5 interaction led to occasional HC loss (Figure 3K) and to stereocilia degeneration in OHCs and stereocilia fusion in IHCs (Figures 3L and M), which might explain why expression of the truncated proteins resulted in hearing loss. Together, these results suggest that, although peptides 5 and 6 interact with Clic5, the cause of hearing loss is not related to CLIC5. Also, we further demonstrated that the ring structure is still detectable in PTPRQ or CLIC5 staining by deleting the $TPRN^{105\text{-}506}$, while no rings of TPRN were observed (Figure S2). Taken together, we propose that the TPRN rings are necessary for stabilizing the stereocilia and therefore for normal hearing.

The dose of expressed TPRN is crucial for TPRN rings formation and auditory function

We next generated $Tprn^{\Delta/\Delta}$ mice by deleting all of the *Tprn* exons using the CRISPR-Cas9 system (Figure S3A) to partially evaluate the effect of TPRN ring deficiency in HCs. Immunostaining showed that TPRN was completely absent in HCs in $Tprn^{\Delta/\Delta}$ mice (Figure S3B). We analyzed the hearing ability of $Tprn^{\Delta/\Delta}$ mice by ABR and found that adult $Tprn^{\Delta/\Delta}$ mice showed almost complete deafness (Figure 4A) with slight to severe HC loss with aging (Figure S3C). High-magnification SEM images showed that hair bundles in OHCs were disordered in the apical region of the cochlea and that stereocilia were missing in the middle and basal regions of the cochlea in $Tprn^{\Delta/\Delta}$ mice (Figures 4B and 4C). In addition, fused stereocilia were observed in IHCs (Figure 4D). To exclude the possibility that genomic elements in the deleted region of $Tprn^{\Delta/\Delta}$ mice might contribute to the phenotype, we designed shRNAs to knockdown *Tprn* mRNA in the HCs of wild-type mice. The knockdown efficiencies of *Tprn* shRNAs were validated by western blotting and immunofluorescence (Figures S4A and S4B). Next, validated *Tprn*-shRNA was packaged into Anc80L65 with the red fluorescence protein Scarlet[38] under the control of a CAG promoter. Using RWM injection, we delivered *Tprn*-shRNA and scrambled-shRNA into the cochleae of P3 mouse pups. The infection efficiency was indicated by Scarlet fluorescence. Compared with the scrambled-shRNA group, only faint TPRN protein signals could be detected in the HCs of the *Tprn*-shRNA group (Figure S4C). The ABR thresholds were significantly increased in the *Tprn*-shRNA-injected mice compared with the controls (Figure S4D). Taken together, our results indicate that TPRN rings are crucial for normal hearing ability.

Furthermore, we found that the overexpression of TPRN affected normal hearing in a dose-dependent manner. We injected different amounts of genomic copies (GCs) of Anc80L65-*Tprn*-HA (0.75×10^9 GCs, 1.5×10^9 GCs, and 4×10^9 GCs) into wild-type mice to evaluate changes in hearing thresholds and TPRN rings. Higher transduction rates of HCs were observed with increased dose of AAV-*Tprn* (Figures S5A and S5B), and the ABR results showed that mice injected with different titers of virus all showed increased hearing thresholds at all frequencies, and the thresholds became higher as the amount of virus increased (Figures 4E and 4F). The STED images showed that, in exogenous

(H) Representative confocal images of stereocilia injected with Anc80L65-*Tprn* no. 5-HA. Cyan, phalloidin; red, *Tprn* no. 5-HA. Scale bar, 1 μm. (I) Representative ABR traces recorded from control, Anc80L65-*Tprn* no. 5-HA-injected, and Anc80L65-*Tprn* no. 6-HA-injected mice, with a 16 kHz tone burst between 20 and 90 dB. (J) ABR results of control (n = 4), Anc80L65-*Tprn* no. 5-HA-injected (n = 6), and Anc80L65-*Tprn* no. 5-HA-injected (n = 6) mice, and statistical analyses was performed between control and Anc80L65-*Tprn* no. 5 or no. 6-HA-injected ears. (K) SEM images of cochlear epithelia from control and Anc80L65-*Tprn* no. 5-HA-injected mice. Yellow triangles indicate the missing HCs. Scale bar, 10 μm. (L) SEM images of stereocilia from control and Anc80L65-*Tprn* no. 5-HA-infected HCs at day 35 after surgery at P2. Yellow arrows indicate the missing stereocilia. Scale bar, 1 μm. (M) The total stereocilia counts in control and Anc80L65-*Tprn* no. 5-HA-infected OHCs corresponding to (L). Error bars are the standard error of the mean. The p value was calculated by Student's t test or one-way ANOVA. *$p < 0.05$, **$p < 0.01$, ***$p < 0.001$.

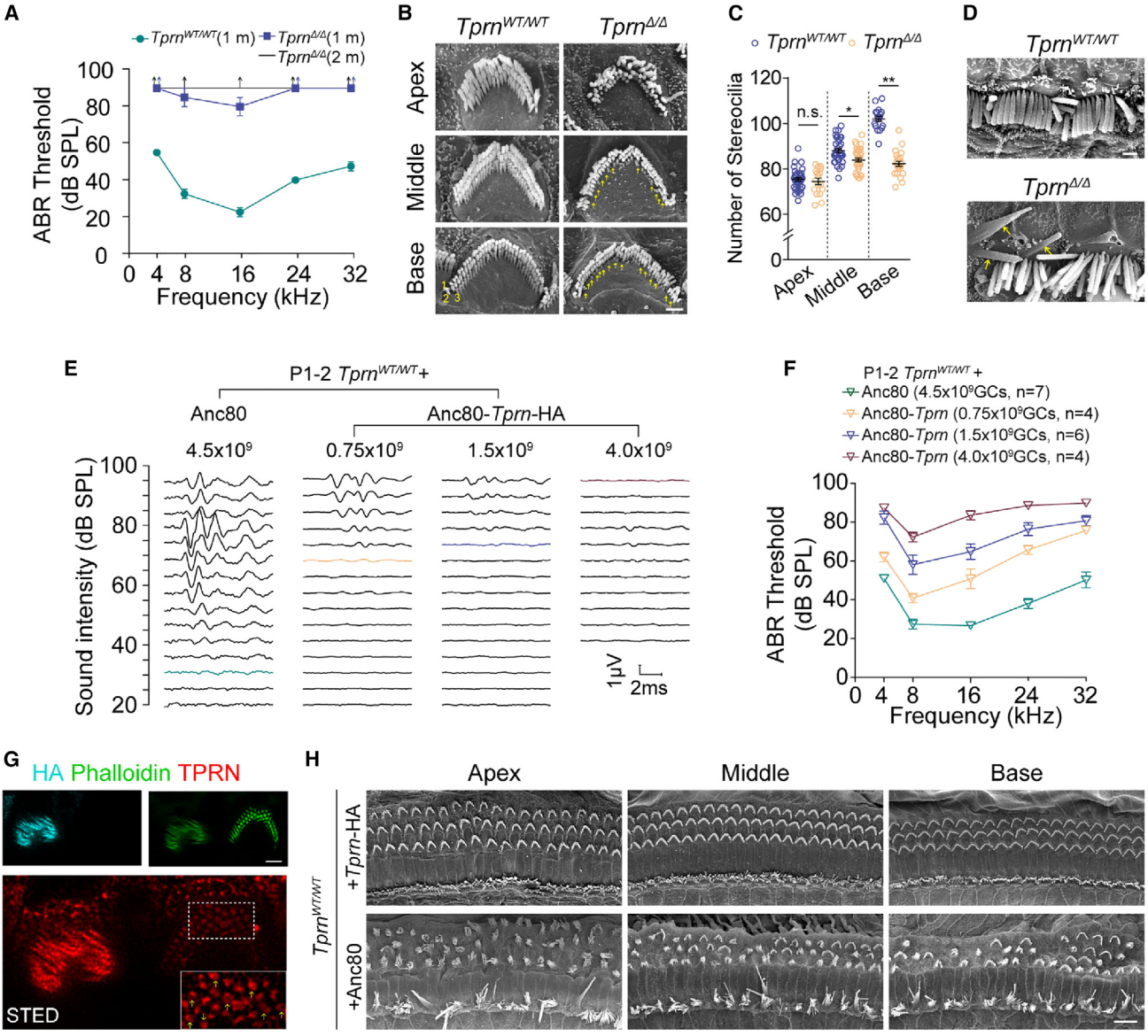

Figure 4. The alterable TPRN expression levels lead to disrupted TPRN rings, degenerative stereocilia, and severe hearing loss

(A) ABR results of *Tprn*$^{WT/WT}$ (wild-type mice, 1-month, n = 3), *Tprn*$^{\Delta/\Delta}$ (1-month, n = 5), and *Tprn*$^{\Delta/\Delta}$ (2-month, n = 3) mice. (B) Representative SEM images of stereocilia in OHCs from control and *Tprn*$^{\Delta/\Delta}$ mice at P30. Numbers 1–3 represent the rows of stereocilia from tall to short. Yellow arrows indicate the missing stereocilia. Scale bar, 1 μm. (C) The total stereocilia count in *Tprn*$^{WT/WT}$ and *Tprn*$^{\Delta/\Delta}$ OHCs at P30. (D) SEM images of stereocilia in IHCs from *Tprn*$^{WT/WT}$ and *Tprn*$^{\Delta/\Delta}$ mice at P30. Yellow arrows indicate the fused stereocilia. Scale bar, 2 μm. (E) Representative ABR traces recorded from Anc80 and different titers of Anc80-*Tprn*-HA-injected *Tprn*$^{WT/WT}$ mice at P30 with a 16 kHz tone burst between 20 and 90 dB. (F) ABR results from *Tprn*$^{WT/WT}$ mice injected with Anc80 and different doses of Anc80L65-*Tprn*-HA at P30. (G) Representative STED image of TPRN (red) in stereocilia from an Anc80L65-*Tprn*-HA-infected OHC. The inset is the magnified region of the dashed box and the brightness of the TPRN signal is linearly adjusted. AAV-TPRN is indicated by the HA (cyan) staining, and the stereocilia were stained by phalloidin (green). Scale bar, 2 μm. (H) Representative SEM images of the cochlear epithelia from *Tprn*$^{WT/WT}$ mice injected with control Anc80L65 and Anc80L65-*Tprn*-HA at a dose of 7.5×10^9 GCs, respectively. Scale bar, 10 μm. Error bars are the standard error of the mean. The p value was calculated by Student's t test. n.s., no significant difference. *$p < 0.05$, **$p < 0.01$.

TPRN-HA-expressed HCs, TPRN signals were stronger and dispersed along the entire shaft of the stereocilium with no detected TPRN rings, while obvious TPRN rings could be observed in the HCs without AAV-*Tprn* transduction (Figure 4G). Also, the stereocilia looked disorganized in the TPRN overexpressed HCs compared with those in the AAV-negative HCs (Figures 4H and S5A), with more HC loss detected in the AAV-*Tprn*-injected cochlea at a dose of 4×10^9 GCs (Figure S5C). Taken together, these observations indicate that TPRN rings anticipate the architecture maintenance of stereocilia and normal hearing function.

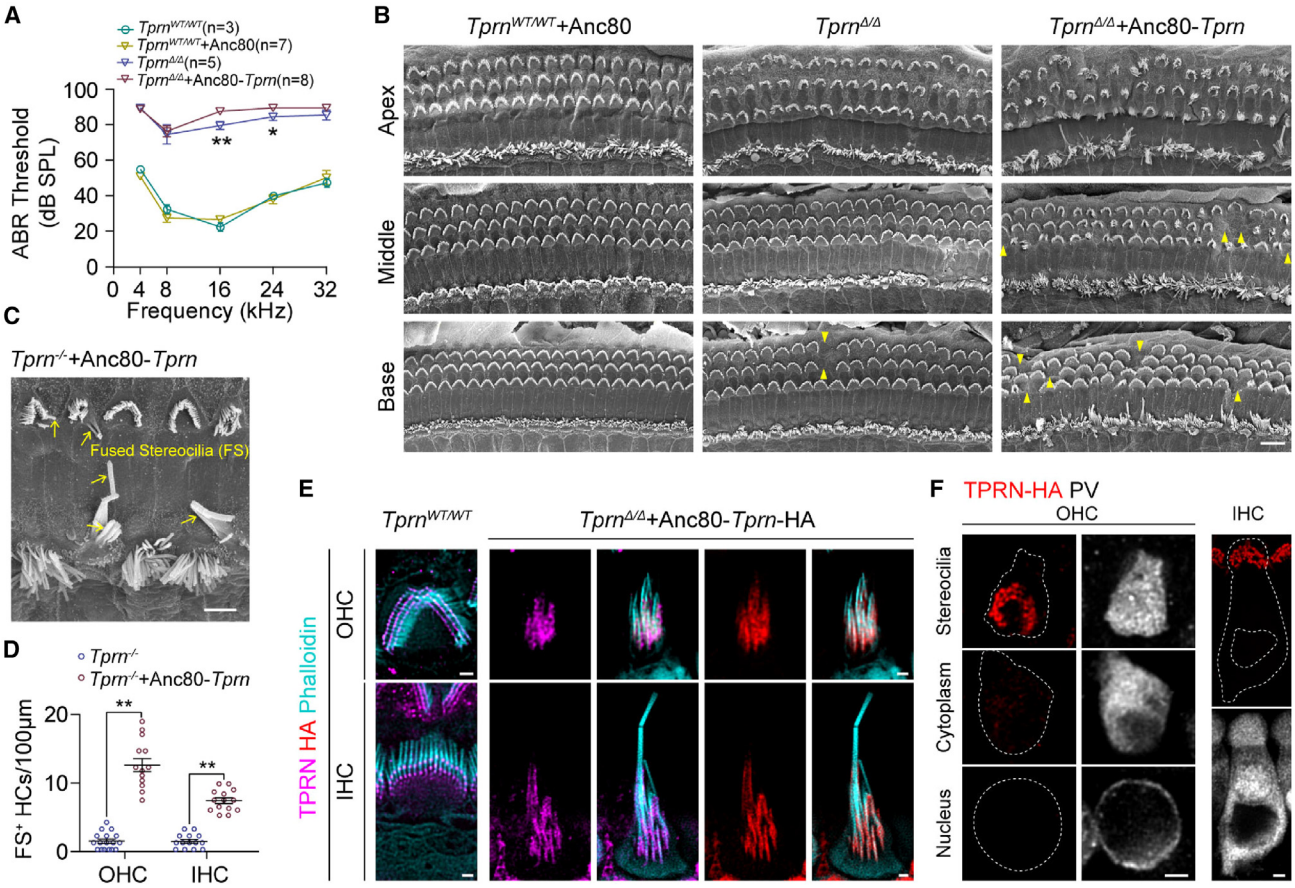

Figure 5. The massive overdose of TPRN was not capable of restoring impaired hearing in *Tprn*$^{\Delta/\Delta}$ mice

(A) ABR results of *Tprn*$^{WT/WT}$ mice, *Tprn*$^{WT/WT}$ mice injected with empty vector (*Tprn*$^{WT/WT}$ + Anc80), *Tprn*$^{\Delta/\Delta}$ mice, and *Tprn*$^{\Delta/\Delta}$ mice injected with exogenous *Tprn*-HA (*Tprn*$^{\Delta/\Delta}$ +Anc80-*Tprn*), respectively. All mice were injected with virus at P1–P2 at a dose of 4.5 × 10^9 GCs and harvested after 4 weeks. The statistical differences were analyzed between *Tprn*$^{\Delta/\Delta}$ and *Tprn*$^{\Delta/\Delta}$ + Anc80-*Tprn* mice. (B) Representative SEM images of cochlear epithelia from *Tprn*$^{\Delta/\Delta}$, *Tprn*$^{\Delta/\Delta}$ + Anc80, and *Tprn*$^{\Delta/\Delta}$ + Anc80-*Tprn* mice at 4 weeks after surgery at P2. Yellow triangles indicate the missing OHCs. Scale bar, 10 μm. (C) Magnified SEM images from (B). Yellow arrows indicate the fused stereocilia (FS). Scale bar, 5 μm. (D) Fused stereocilia counting in *Tprn*$^{\Delta/\Delta}$ and *Tprn*$^{\Delta/\Delta}$ + Anc80L65-*Tprn* HCs. (E) Representative confocal images of exogenous TPRN signals in stereocilia from *Tprn*$^{WT/WT}$ and *Tprn*$^{\Delta/\Delta}$ + Anc80-*Tprn* infected HCs. Cyan: F-actin, magenta: TPRN, red: HA. Scale bars, 1 μm. (F) The localization of the exogenous TPRN-HA signal in OHC and IHC from *Tprn*$^{\Delta/\Delta}$ + Anc80L65-*Tprn*-HA mice. Red, HA; gray, parvalbumin (PV), an HC marker. Scale bars, 2 μm. Error bars are the standard error of the mean. The p value was calculated by Student's t test. **p < 0.01.

Lower expression of TPRN partially restores the hearing function of *Tprn* deficiency mice

To further investigate the role of TPRN rings in hearing, we re-expressed TPRN in *Tprn*$^{\Delta/\Delta}$ mice to evaluate the restoration of auditory function. RWM injection of Anc80L65-CAG-*Tprn*-HA was performed at P0-P1 and the ABRs were measured at P30, a stage at which *Tprn*$^{\Delta/\Delta}$ mice showed profound deafness (Figure 4A). Unexpectedly, the injected mice showed more serious hearing loss at medium and high frequencies compared with the control mice (Figure 5A). The stereocilia in AAV-*Tprn*-injected HCs from *Tprn*$^{\Delta/\Delta}$ mice seemed to be more disordered along the whole cochlea than in untreated *Tprn*$^{\Delta/\Delta}$ mice by SEM imaging, and greater HC loss was seen in treated *Tprn*$^{\Delta/\Delta}$ mice (Figures 5B–5D).

We wondered why *Tprn* overexpression not only failed to rescue hearing loss but exacerbated the damage to the auditory epithelia in *Tprn*$^{\Delta/\Delta}$ mice. We speculated that the expression level of exogenous TPRN under the control of the CAG promoter (an enhanced promoter that drives strong expression of the target gene) was too high to function correctly. Considering that endogenous TPRN was only obviously detected in the taper region, we imaged the exogenous *Tprn*-HA signal and found that TPRN and HA signals were detected along the whole shaft of the stereocilium rather than in the taper region (Figure 5E), which was similar to that in AAV-*Tprn*-transduced HCs in wild-type mice and thus might lead to the defects in the stereocilia. In addition, we observed barely any TPRN-HA signals in the cytoplasm or nucleus of HCs in three-dimensional stack images (Figure 5F), indicating that exogenous TPRN was mostly transported to the stereocilia. Therefore, these results verified our speculation that the misallocation of exogenous TPRN in the stereocilia by overexpression in *Tprn*$^{\Delta/\Delta}$ mice caused the more severe collapse of stereocilia and increased hearing loss.

The heterozygous mice ($Tprn^{WT/\Delta}$) with an insufficient haplo-dose of *Tprn* showed normal hearing and normal sensory epithelia morphology with TPRN rings in the stereocilia (Figure S6), which means that small amounts of the TPRN molecules maintain TPRN rings and normal hearing. We tried to significantly reduce the amount of exogenous TPRN by using HHR. HHR is a type of small self-cleaving ribozymes that is widely used in the reversible cleavage of transcriptional RNA in order to regulate gene expression.[39] According to a previous study, the type I HHR N107v1 resulted in the 34-fold inhibition of the Gaussian luciferase reporter gene in HEK293T cells.[40] The introduction of N107v1 at the 3′ UTR of the exogenous *Tprn* gene (Figure 6A) might be able to reduce gene expression in the cochlea and thus restore hearing. We delivered exogenous *Tprn* along with N107v1 at the 3′ UTR by Anc80L65 injection into the cochleae of P1-P2 $Tprn^{\Delta/\Delta}$ mice (Figure 6A). The TPRN-HA expression and hearing thresholds of virus-injected $Tprn^{\Delta/\Delta}$ mice were measured 30 days later. TPRN was successfully expressed in the hair bundles at around P30 (Figure 6B). ABR experiments showed that several $Tprn^{\Delta/\Delta}$ mice injected with low-dose N107v1 (6×10^9 GCs) had improved hearing thresholds (Figures 6C and 6D) with the greatest rescue of about 30 dB in the middle frequencies (Figure 6C), and about half of the injected $Tprn^{\Delta/\Delta}$ mice showed varying degrees of hearing recovery at different frequencies (Figure 6D).

We thus evaluated the expression of *Tprn* in the *Tprn*-N107v1-injected mice at both the transcriptional and translational levels. The Anc80-*Tprn*-N107v1-injected cochlea and the contralateral cochlea showed fewer *Tprn* mRNA transcripts compared with the Anc80-*Tprn*-injected mice, with approximately 100- and 3-fold inhibition, respectively (Figure 6E). Besides, the expression level of *Tprn* in the injected cochlea was more than 15-fold greater than that in contralateral cochlea (Figure 6F). Similar tendencies were verified by western blotting and immunostaining of TPRN-HA at the translational level (Figures 6G and 6H). More importantly, TPRN-HA at a lower expression level in the $Tprn^{\Delta/\Delta}$ mice showed the ring-like structure again (Figure 6I), indicating that the restoration of the ring structure of TPRN might be the basis of hearing recovery. This also indicated the importance of the ring structure in the maintenance of normal hearing. Also, the reduced exogenous TPRN in HCs driven by a weaker promoter CMV173[41,42] partially lowered the hearing threshold and restored the hearing with the greatest rescue of about 30 dB in the middle frequencies (Figures 6J–6M). Taken together, these results suggest that moderate amounts of exogenous TPRN via HHR and Anc80L65 virus in HCs at early developmental stages can reproduce the disrupted rings and restore hearing ability. The use of HHR or weaker promoter is expected to achieve a therapeutic effect without introducing strong cytotoxicity in disease treatments, thus improving the safety and effectiveness of gene therapy.

DISCUSSION

Super-resolution imaging methods have been widely used to obtain high spatial resolution images to analyze protein distributions in cellular compartments and the interactions between compartments. Here, STED imaging revealed a remarkably regular organization, with TPRN forming ring-like structures with diameters of 160–170 nm in OHCs and 190–200 nm in IHCs, thus providing important insights into TPRN structure and function *in situ*. Similarly, Fam65b, another vital protein in the taper region of stereocilia, also forms ring-like structures,[31] and our previous study found that spectrin and actin can form ring-like structures in the cuticular plate of HCs.[30,43] Here, we also observed the ring-like structures of PTPRQ and CLIC5 (Figure 2). Together, these results suggest that ring-like structures may be common in HCs. Notably, Zhao et al. detect a solid structure of TPRN in IHCs rather than the ring-like structure by using STORM, which is another super-resolution fluorescence method.[31] We believe that STORM is superior when used on cultured cells[44] but that it has some limitations when used on tissues, especially in the case of semi-intact preparations like the dissected cochlea. This is due in part to the tissue yielding high background noise relative to the single molecule image, which leads to diminished spatial resolution. Most importantly, we verified our results by TPRN-HA knockin strategy (Figures 1 and S1), which ruled out any effects of the TPRN antibody. Thus, we believe that TPRN indeed forms a ring-like structure, but how the ring-like structure is formed and why TPRN protein is restricted to the taper region are unknown.

Previous studies have suggested that TPRN might be a member of a membrane-associated protein complex including PTPRQ, CLIC5, radixin, and MYO6.[18] In *Clic5*-deficient mouse HCs, TPRN and radixin diffused along the shaft of the stereocilia with no change in expression at the transcriptional level. [18] CLIC5 has been shown to bind directly to TPRN18, and we also confirmed this result (Figure 2A). Our data also showed that TPRN has a strong binding affinity for actin and PTPRQ (Figures 1H and 2E). Also, researchers have confirmed that CLIC5 can interact with GRXCR219. All of these interactions indicate that PTPRQ, CLIC5, TPRN, MYO6, GRXCR2, and actin may form a large protein complex in the taper region. Moreover, we observed the ring-like structures of PTPRQ and CLIC5 (Figure 2), which may partially explain how the TPRN ring-like structure is formed in the taper region.

As a special structure for resisting mechanical stress, the taper region is crucial for the proper functioning of stereocilia.[3,45,46] Mutations in many proteins enriched in or near the taper region lead to severe hereditary hearing loss.[9–16] In this study, we found that several proteins in this region can form ring-like structures, which may also be important for proper stereocilia function and thus for hearing. The lack of CLIC5 causes submembrane TPRN to diffuse along the whole length of the stereocilia and leads to stereocilia defects.[17] Disruption of the structure of TPRN rings results in severe stereocilia disorders and deafness with no defects on the CLIC5 or PTPRQ rings (Figure 3). TPRN rings may be involved in the maintenance of stereocilia by other pathways. Interestingly, in the ClinVar database, three out of seven TPRN mutations in patients are located in the identified interaction region, suggesting that disruption of the ring-like structure may be the mechanism underlying the hearing loss caused by these three mutations.

In addition to its location and structure, the expression level of TPRN is also critical for its proper function. Our study reflects that the

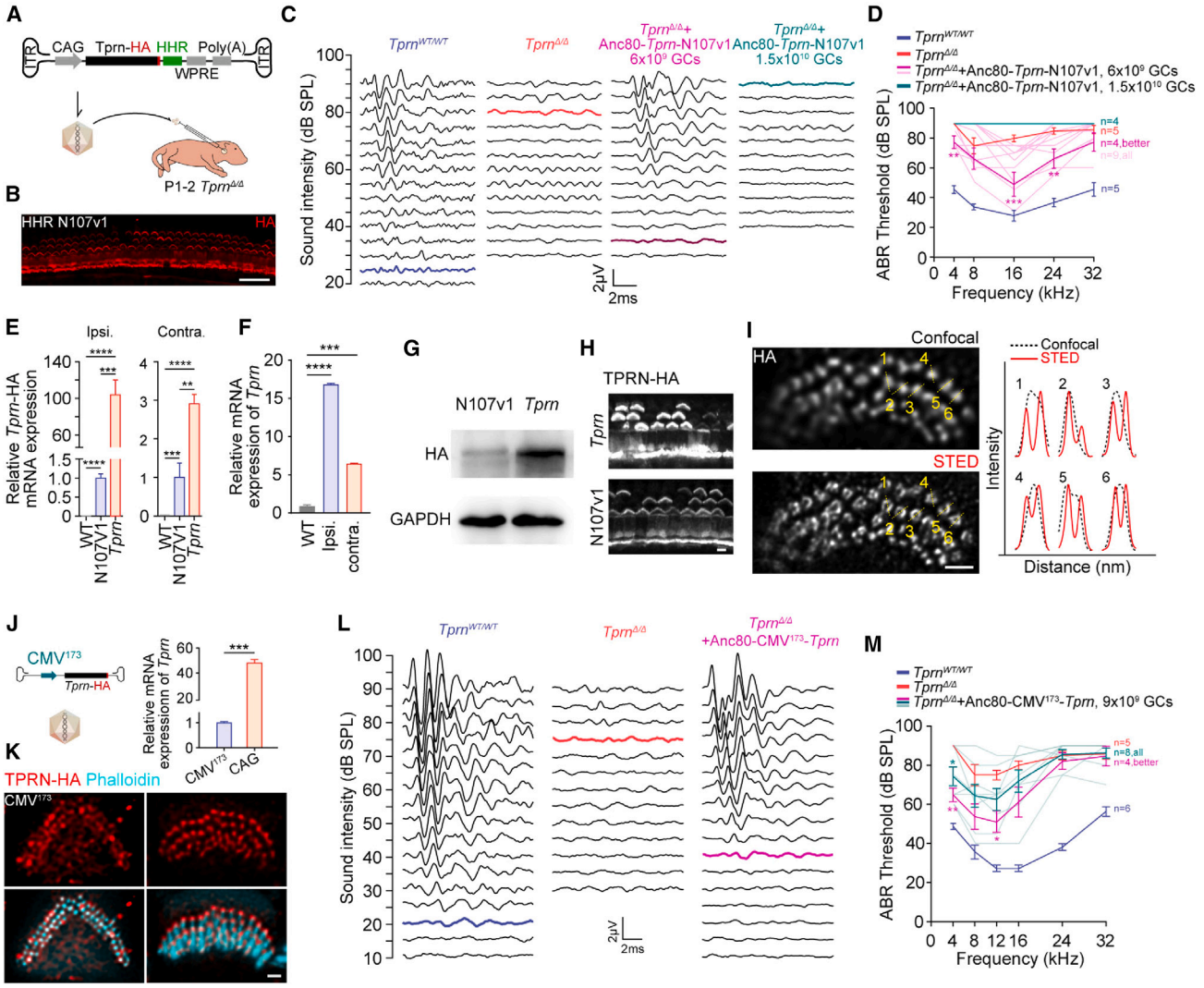

Figure 6. Lower exogenous TPRN expression partially restored impaired hearing in *Tprn*$^{\Delta/\Delta}$ mice

(A) Diagram of the HHR-mediated expression of exogenous *Tprn*-HA in P1-2 *Tprn*$^{\Delta/\Delta}$ mice. (B) Representative confocal images of TPRN-HA signals (red) in the cochlear epithelia from Anc80-*Tprn*-HA-HHR N107v1-injected *Tprn*$^{\Delta/\Delta}$ mice at P30. Scale bar, 20 μm. (C) Representative ABR traces recorded from P30 mice of *Tprn*$^{WT/WT}$, *Tprn*$^{\Delta/\Delta}$, *Tprn*$^{\Delta/\Delta}$ + Anc80-*Tprn*-N107v1 (6 × 10^9 GCs), and Tprn$^{\Delta/\Delta}$ + Anc80-*Tprn*-N107v1 (1.5 × 10^{10} GCs) with a 16 kHz tone burst between 20 and 90 dB. (D) The corresponding ABR results at different frequencies are shown, and statistical analysis was between untreated (*Tprn*$^{\Delta/\Delta}$) and Anc80-*Tprn*-HA-N107v1-treated *Tprn*$^{\Delta/\Delta}$ ears. (E) qPCR results of *Tprn*-HA expression at the transcriptional level from WT control, Anc80-*Tprn*-HA-N107v1 (N107v1, 6 × 10^9 GCs)- or Anc80-*Tprn*-HA (*Tprn*, 6 × 10^9 GCs)-injected cochleae and the contralateral cochleae. (F) qPCR results of *Tprn*-HA expression at the transcriptional level from WT control, Anc80-*Tprn*-HA-N107v1 (6 × 10^9 GCs)-injected cochlea (ipsilateral) and the contralateral cochleae. (G) Representative images of TPRN-HA immunostaining by western blot. Protein samples were collected from cochleae injected with Anc80-*Tprn*-HA-N107v1 (6 × 10^9 GCs) or Anc80-*Tprn*-HA (6 × 10^9 GCs). (H) Representative confocal images of TPRN-HA (gray) signals in the cochlear epithelia from *Tprn*$^{\Delta/\Delta}$ mice injected with Anc80-*Tprn*-HA-N107v1 (N107v1, 6 × 10^9 GCs) or Anc80-*Tprn*-HA (*Tprn*, 6 × 10^9 GCs). Scale bar, 5 μm. (I) Conventional confocal and STED images of TPRN-HA in a rescued IHC. The intensity profiles corresponding to the dashed lines (1–6) are shown to the right. Scale bar, 1 μm. (J) Diagram of the promoter CMV173-mediated expression of exogenous TPRN-HA in P1-2 *Tprn*$^{\Delta/\Delta}$ mice; and the qPCR results of *Tprn* expression at the transcriptional level from Anc80-CMV^{173}-*Tprn*-HA- and Anc80-CAG-*Tprn*-HA-injected cochlea at the same dose. (K) Representative confocal images of TPRN-HA (red) and phalloidin (cyan) signals in the cochlear epithelia from *Tprn*$^{\Delta/\Delta}$ mice injected with Anc80-CMV173-*Tprn*-HA (9 × 10^9 GCs). Scale bar, 1 μm. (L) Representative ABR traces recorded from P30 *Tprn*$^{\Delta/\Delta}$ mice injected with Anc80-CMV173-*Tprn*-HA (9 × 10^9 GCs) with a 16 kHz tone burst between 10 and 90 dB. (M) The corresponding ABR results at different frequencies are shown, and statistical analysis was between untreated (*Tprn*$^{\Delta/\Delta}$) and Anc80-CMV173-*Tprn*-HA-treated *Tprn*$^{\Delta/\Delta}$ ears. All mice were injected with virus in the left ear at P1-P2. qPCR and western blotting data were collected at P8-P9. Confocal images and ABR were collected at P30-P32. Error bars are the standard error of the mean. The p value was calculated by Student's t test or one-way ANOVA. *p < 0.05, **p < 0.01, ***p < 0.001, ****p < 0.001.

translated number of TPRN molecules needs to be maintained within a reasonable range. The study shows that the stereocilia defects in Grxcr2 mutant mice were caused by the mis-localization of TPRN proteins, which was relieved by the translational reduction of TPRN.[17] Here, we used Anc80L65 for exogenous TPRN expression in the cochlea *in vivo* at P1 through RWM injection. The moderate overexpression of exogenous TPRN profoundly affected the therapeutic effect (Figure 5). When choosing the isotypes of HHR, N79 was also a candidate variant. N79-mediated gene expression resulted in a 16-fold reduction of Gaussian luciferase reporter gene expression in HEK293T cells.[40] However, our ABR experiments showed that both low-dose and high-dose N79 injection (6×10^9 GCs and 1.5×10^{10} GCs) in $Tprn^{\Delta/\Delta}$ mice were ineffective at alleviating impaired hearing (Figure S7). In fact, depleting one allele of *Tprn* in the genome had no effect on the auditory epithelia or on normal hearing (Figure S6), indicating that a small amount of exogenous TPRN may also restore hearing. This is why HHR N107v1/CMV[173]-mediated *Tprn* delivery could rescue hearing loss. Also, because of the high infection efficiency of Anc80L65 in utricular HCs from adult humans, AAV-mediated gene therapy has promise for the clinical treatment of progressive hereditary hearing loss.

A critical discussion in this study is the safety and efficacy of ubiquitous promoters. In addition to the potential genotoxicity caused by the introduction of stronger gene re-expression, ubiquitous promoters such as the CAG promoter can also cause hearing damage in adult mice.[47] Cell-specific promoters tend to express proteins with weak activity and may be applicable in this type of gene therapy studies that do not require high expression of exogenous proteins. Currently, there are no published studies utilizing specific promoters for gene therapy inherited deafness in mice. However, according to publicly available information, in the DB-OTO, an AAV gene therapy drug developed by Decibel Therapeutics that targets the OTOF is driven by the HC-selective *Myo15* promoter. Preclinical studies in OTOF mutant mice demonstrated that DB-OTO administration resulted in sustained improvement in auditory function for up to nearly 1 year. Studies in non-human primates demonstrated full-length expression of OTOF driven by *Myo15* promoter in the cochlear basilar membrane. The above study fully illustrated the effective application of HC-specific promoters in deafness gene therapy. This is an important and promising research direction that deserves in-depth exploration.

In summary, we have identified the role of TPRN in cochlear structure and function. We characterized the organization and pattern of TPRN-CLIC5-PTPRQ within the stereocilia using super-resolution imaging methods and showed that these proteins form ring-like structures corresponding to each stereocilium. Within the structures, the proper spatial organization of TPRN rings in the stereocilia appears to play a critical role in stereocilia stabilization and hearing function in a dose-dependent manner. Ring disruption leads to impaired hearing. In addition, TPRN could partially restore impaired hearing, providing further support for the development of viral gene transfer in the inner ear for treating sensory HC disorders caused by *TPRN* mutation.

MATERIALS AND METHODS

Animals

C57BL/6 mice and $Tprn^{\Delta/\Delta}$ mice of both genders were used in this research. The day of birth was determined as P0. The genotyping primers for $Tprn^{\Delta/\Delta}$ mice are listed in Table S1. Animals were housed under a 12 h light/dark cycle at 22°C ± 1°C with food and water available *ad libitum*. All experiments were approved by the Institutional Animal Care and Use Committee of Southeast University and ShanghaiTech University, China.

Immunofluorescence

The temporal bone was rapidly dissected out of the mouse pups. The cochlear spiral was micro-dissected from the temporal bone and adhered to a slide cover glass coated with tissue-adhesive Cell Tak (BD Bioscience) in cold PBS (pH 7.2). Cochleae were fixed with 4% paraformaldehyde in PBS (pH 7.2) at room temperature for 1 h. For cochleae from mice older than P7, the temporal bone was fixed with 4% paraformaldehyde in 1× PBS (pH 7.2) for 2 h at room temperature before being cut into pieces after 0.5 mM EDTA (pH 8.0) treatment. For cultured cells, cells were fixed with 4% paraformaldehyde in PBS (pH 7.2) at room temperature for 30 min. Samples were immersed in blocking medium containing 10% donkey serum and 0.5% Triton X-100 in PBS (pH 7.2) for 1–2 h at room temperature and then incubated with primary antibodies overnight followed by secondary antibodies conjugated with Alexa Fluor dyes. The primary antibodies were TPRN (rabbit, Sigma-Aldrich), myosin7a (rabbit, Proteus Bioscience), parvalbumin (mouse, Swant), and HA (rat, Roche). The secondary antibodies were conjugated with Alexa Fluor-conjugated IgG (H + L) (1:500 dilution; Thermo Fisher Scientific). Atto 488-conjugated phalloidin (1:1,000 dilution; ATTO-TEC) was used to label actin, and DAPI (1:10,000 dilution; Thermo Fisher Scientific) was used to label DNA.

STED imaging

STED images were acquired with a Leica TCS SP8 STED 3× microscope equipped with a white light pulse laser (WLL2), STED depletion lasers (592 and 660 nm were used in this study), an oil immersion 100×/NA 1.4 objective lens (HC PL APO CS2, Leica), and a TCS SP8 time-gated system. Images (1,024 × 1,024 pixels) were obtained in confocal mode or STED mode. Acquisition settings were optimized to obtain high-quality images, including laser power, image size, scanning speed, frame accumulation, and time-gating interval. Deconvolution of STED images was performed with Huygens software (Scientific Volume Imaging) using the Huygens classical maximum likelihood estimation deconvolution algorithm or the Lighting software (Leica).

Plasmid construction and transfection, coIP, and western blotting

Target cDNA sequences were cloned from mouse cochlear cDNA using Phanta Max Super-Fidelity DNA Polymerase (Vazyme) or were synthesized by GenScript. Sequences were constructed into corresponding vectors containing fluorescent proteins, and the C termini of target proteins were linked to a 3× FLAG tag or a 3× HA tag

for further coIP. coIP was performed in mouse N2A cells (American Type Culture Collection) or human HEK293T cells (American Type Culture Collection). Cells were cultured in Dulbecco's modified Eagle's medium plus GlutaMAX (Thermo Fisher Scientific) supplemented with 10% (v/v) fetal bovine serum and 100 U/mL penicillin/streptomycin (Thermo Fisher Scientific) at 37°C with 5% CO_2. Cells were homogenized in lysis buffer (50 mM Tris, 120 mM NaCl, and 0.5% NP40) containing a mixture of protease inhibitors (Roche) and PMSF (Sigma). After centrifugation, the protein supernatant was incubated with Anti-FLAG M2 magnetic beads (mouse, Sigma) at 4°C overnight. After immunoprecipitation, the protein samples were separated on SDS-PAGE gels (Bio-Rad) and transferred to nitrocellulose filter membranes (0.45 μm, Millipore, Billerica, MA). The membranes were blocked with 5% nonfat dry milk for 2 h at RT and incubated overnight at 4°C with primary antibodies. The following first antibodies were used in this study: FLAG (rabbit, Proteintech), β-actin (rabbit, Abcam), and HA (rabbit, Proteintech). Then, the membranes were then incubated with HRP-conjugated secondary antibody (1:10,000 dilution; Santa Cruz) for 2 h at room temperature. Signals were visualized using an enhanced chemiluminescence kit (Pierce) and captured with an ImageQuant LAS4000 (GE Healthcare Bioscience). Immunoprecipitation experiments were repeated at least two times to verify the reproducibility of the data.

AAV

The target sequence was integrated into Anc80L65 containing the cytomegalovirus enhancer/chicken β-actin promoter[48] and the woodchuck hepatitis virus post-transcriptional regulatory element (WPRE) cassette flanked by AAV2 inverted terminal repeats. AAV production,[49] purification,[50] and titration[51] were performed as previously reported. Anc80L65 was produced in HEK293T cells and purified by iodixanol gradient ultracentrifugation. In brief, culture medium and HEK293T cells were collected at 96 h after plasmids were co-transfected. Culture medium was concentrated by precipitation with 10% PEG 8000 (Sigma) and 1.0 M NaCl (Sigma), and the cell lysate was treated with 1 mM $MgCl_2$ (Thermo Fisher Scientific) and 0.25 mM KCl (Thermo Fisher Scientific). DNase I (10 U/mL, Thermo Fisher Scientific) and RNase I (10 U/mL, Thermo Fisher Scientific) were added to the combined mixture for 1-h incubation at 37°C. After centrifugation, the Anc80L65 in the clarified supernatant was purified by gradient iodixanol gradient (15%, 25%, 40%, and 60%) ultracentrifugation. The GC titers of Anc80L65 were determined by SYBR (Roche)-based qPCR analysis using primers targeting the WPRE region with linearized genome plasmids as the standard. The primers are listed in Table S1.

RWM injection

P0-P2 mouse pups were injected with corresponding AAVs via the RWM using a microinjection spring needle as previously described.[33] RWM injection was performed only on the left ear of each animal. Mice pups were anesthetized in an ice bath for 2–3 min and then put on a cold pad for subsequent surgical procedures. Upon anesthesia, a post-auricular incision was made to expose the otic bulla and visualize the round window in the cochlea after degerming with iodine and 70% ethanol. Injections were performed with a glass micropipette controlled by a micromanipulator UltraMicroPump (UMP3, World Precision Instruments). Approximately 1–1.5 μL of virus at proper concentration was manually injected for 1 min. After injection, the skin incision was closed by daubing veterinary tissue adhesive (Millpledge) at the surgery site on the skin. The entire procedure took less than 5 min, and the mouse pups were returned to the 38°C warming pad for 10–15 min and then placed back with their mother for continued nursing.

ABR audiometry

Open-field ABR thresholds were assessed with a Tucker-Davis Technology system III (Tucker-Davies Technologies). After anesthetized with pentobarbital sodium (100 mg/kg) intraperitoneally, mice were placed on a 37°C heating pad to maintain their body temperature. ABRs were recorded by using needle electrodes placed over the scala to record the changes in the electrical activity of the brain in response to sound. The ABR responses were elicited in tone bursts between 10 and 90 dB (decibels SPL) at frequencies of 4, 8, 16, 24, and 32 kHz. Acquired response signals collected by the electrodes were amplified 10,000 times, filtered at 0.1–2 kHz, averaged 512–1,024 times, and presented using BioSigRZ software (Tucker-Davies Technologies).

SEM imaging

The temporal bone was rapidly dissected out in cold PBS (pH 7.2). A hole was dug into the apical region of the temporal bone, and fresh 2.5% glutaraldehyde in PBS (pH 7.2) was infused from the hole into the cochlear duct. The cochleae were incubated in the fixative solution at 4°C overnight. After decalcifying in 0.5 M EDTA (pH 8) at room temperature for 6–10 h, the cochlear specimens were dissected into pieces and immersed in 2% osmium tetroxide for post-fixing for 3 h at 4°C. After washing three times in ultrapure water, the samples were dehydrated through a graded ethanol series (30%, 50%, 70% 90%, and 100%). Each step lasted 10 min. The samples were critical-point dried (Leica, EMCPD300) and then placed carefully onto a piece of conductive cloth tape and sputter-coated with 10 nm platinum (JEC-3000FC, JEOL). The morphology was observed with a field emission SEM at 10 kV (JSM-7800F prime, JEOL).

Data analysis

Images were exported in tiff format from origin software and further processed by Fiji software (National Institutes of Health). The brightness and contrast of the entire image were linearly adjusted. For quantitatively analyzing the distribution pattern of TPRN, lines across the immunosignals were drawn and the intensity profiles were measured, and autocorrelation was subsequently analyzed using MATLAB (The MathWorks).

Statistical analysis

Statistical analyses were performed in GraphPad Prism 6.07 software (GraphPad Software). Two-tailed unpaired Student's t test or one-way ANOVA were used to determine the statistical significance of differences. $p < 0.05$ was considered statistically significant.

DATA AND CODE AVAILABILITY

All data associated with this study are present in the paper or the supplemental information.

SUPPLEMENTAL INFORMATION

Supplemental information can be found online at https://doi.org/10.1016/j.ymthe.2023.11.011.

ACKNOWLEDGMENTS

We thank the ShanghaiTech University and the Bioimaging Core Facilities of the iHuman Institute and the animal facility of National Center for Protein Science Shanghai for their financial support. We also thank Prof. Fujun Wu from Southeast University for imaging support. This work was supported by the National Key Research and Development Program of China (2021YFA1101300 to R.C., 2021YFA1101800 to X.C., 2020YFA0113600 to J.Q., and 2020YFA0112503 to R.C.), the STI2030-Major Projects (no. 2022ZD0205400 to J.Q.), the National Natural Science Foundation of China (82330033 to R.C., 82030029 to R.C., 81970882 to R.C., 92149304 to R.C., 82000984 to J.Q., 82371162 to J.Q., and 82371161 to F.T.), the China National Postdoctoral Program for Innovative Talents (BX20200082 to J.Q.), the China Postdoctoral Science Foundation (2020M681468 to J.Q.), the Science and Technology Department of Sichuan Province (2021YFS0371 to R.C.), the Shenzhen Science and Technology Program (JCYJ20190814093401920 to R.C. and JCYJ20210324125608022 to R.C.), 2022 Open Project Fund of Guangdong Academy of Medical Sciences (YKY-KF202201 to R.C.), the Jiangsu Postdoctoral Research Funding Program (2021K156B to J.Q.), and the Fundamental Research Funds for the Central Universities (to J.Q.).

AUTHOR CONTRIBUTIONS

R.C., G.Z., J.Q., and F.T. conceived and designed the experiments. J.Q., F.T., and L.Z. performed most of the experiments. J.Q. acquired the immunofluorescence images and SEM data. F.T. prepared all of the viruses used in this manuscript. J.Q. and L.Z. acquired the AAV-injected data and ABR data. J.Q., L.Z., and F.T. contributed to data analysis. Y.Z., Y.Z., Q.S., N.L., Y.F., X.C., and Y.W. helped with the experiments and data analysis. R.C., G.Z., F.T., and J.Q. discussed the data analysis, interpretation, and presentation and wrote the manuscript with contributions from all authors.

DECLARATION OF INTERESTS

The authors declare no competing interests.

REFERENCES

1. Parker, M., and Bitner-Glindzicz, M. (2015). Genetic investigations in childhood deafness. Arch. Dis. Child. *100*, 271–278.
2. Stamatiou, G.A., and Stankovic, K.M. (2013). A comprehensive network and pathway analysis of human deafness genes. Otol. Neurotol. *34*, 961–970.
3. Barr-Gillespie, P.G. (2015). Assembly of hair bundles, an amazing problem for cell biology. Mol. Biol. Cell *26*, 2727–2732.
4. Gillespie, P.G., and Müller, U. (2009). Mechanotransduction by hair cells: models, molecules, and mechanisms. Cell *139*, 33–44.
5. Bartles, J.R. (2000). Parallel actin bundles and their multiple actin-bundling proteins. Curr. Opin. Cell Biol. *12*, 72–78.
6. Tilney, L.G., Derosier, D.J., Mulroy, M.J., and MULROY, M.J. (1980). The organization of actin filaments in the stereocilia of cochlear hair cells. J. Cell Biol. *86*, 244–259.
7. Crawford, A.C., and Fettiplace, R. (1985). The mechanical properties of ciliary bundles of turtle cochlear hair cells. J. Physiol. *364*, 359–379.
8. Karavitaki, K.D., and Corey, D.P. (2010). Sliding adhesion confers coherent motion to hair cell stereocilia and parallel gating to transduction channels. J. Neurosci. *30*, 9051–9063.
9. Schraders, M., Oostrik, J., Huygen, P.L.M., Strom, T.M., van Wijk, E., Kunst, H.P.M., Hoefsloot, L.H., Cremers, C.W.R.J., Admiraal, R.J.C., and Kremer, H. (2010). Mutations in PTPRQ are a cause of autosomal-recessive nonsyndromic hearing impairment DFNB84 and associated with vestibular dysfunction. Am. J. Hum. Genet. *86*, 604–610.
10. Diaz-Horta, O., Subasioglu-Uzak, A., Grati, M., DeSmidt, A., Foster, J., 2nd, Cao, L., Bademci, G., Tokgoz-Yilmaz, S., Duman, D., Cengiz, F.B., et al. (2014). FAM65B is a membrane-associated protein of hair cell stereocilia required for hearing. Proc. Natl. Acad. Sci. USA *111*, 9864–9868.
11. Ahmed, Z.M., Morell, R.J., Riazuddin, S., Gropman, A., Shaukat, S., Ahmad, M.M., Mohiddin, S.A., Fananapazir, L., Caruso, R.C., Husnain, T., et al. (2003). Mutations of MYO6 are associated with recessive deafness, DFNB37. Am. J. Hum. Genet. *72*, 1315–1322.
12. Khan, S.Y., Ahmed, Z.M., Shabbir, M.I., Kitajiri, S.i., Kalsoom, S., Tasneem, S., Shayiq, S., Ramesh, A., Srisailpathy, S., Khan, S.N., et al. (2007). Mutations of the RDX gene cause nonsyndromic hearing loss at the DFNB24 locus. Hum. Mutat. *28*, 417–423.
13. Weil, D., Küssel, P., Blanchard, S., Lévy, G., Levi-Acobas, F., Drira, M., Ayadi, H., and Petit, C. (1997). The autosomal recessive isolated deafness, DFNB2, and the Usher 1B syndrome are allelic defects of the myosin-VIIA gene. Nat. Genet. *16*, 191–193.
14. Liu, X.Z., Walsh, J., Mburu, P., Kendrick-Jones, J., Cope, M.J., Steel, K.P., and Brown, S.D. (1997). Mutations in the myosin VIIA gene cause non-syndromic recessive deafness. Nat. Genet. *16*, 188–190.
15. Seco, C.Z., Oonk, A.M.M., Domínguez-Ruiz, M., Draaisma, J.M.T., Gandía, M., Oostrik, J., Neveling, K., Kunst, H.P.M., Hoefsloot, L.H., del Castillo, I., et al. (2015). Progressive hearing loss and vestibular dysfunction caused by a homozygous nonsense mutation in CLIC5. Eur. J. Hum. Genet. *23*, 189–194.
16. Imtiaz, A., Kohrman, D.C., and Naz, S. (2014). A frameshift mutation in GRXCR2 causes recessively inherited hearing loss. Hum. Mutat. *35*, 618–624.
17. Liu, C., Luo, N., Tung, C.Y., Perrin, B.J., and Zhao, B. (2018). GRXCR2 Regulates Taperin Localization Critical for Stereocilia Morphology and Hearing. Cell Rep. *25*, 1268–1280.e4.
18. Salles, F.T., Andrade, L.R., Tanda, S., Grati, M., Plona, K.L., Gagnon, L.H., Johnson, K.R., Kachar, B., and Berryman, M.A. (2014). CLIC5 stabilizes membrane-actin filament linkages at the base of hair cell stereocilia in a molecular complex with radixin, taperin, and myosin VI. Cytoskeleton (Hoboken) *71*, 61–78.
19. Li, J., Liu, C., and Zhao, B. (2021). N-Terminus of GRXCR2 Interacts With CLIC5 and Is Essential for Auditory Perception. Front. Cell Dev. Biol. *9*, 671364.
20. Sakaguchi, H., Tokita, J., Naoz, M., Bowen-Pope, D., Gov, N.S., and Kachar, B. (2008). Dynamic compartmentalization of protein tyrosine phosphatase receptor Q at the proximal end of stereocilia: Implication of myosin VI-based transport. Cell Motil. Cytoskeleton *65*, 528–538.
21. Goodyear, R.J., Legan, P.K., Wright, M.B., Marcotti, W., Oganesian, A., Coats, S.A., Booth, C.J., Kros, C.J., Seifert, R.A., Bowen-Pope, D.F., and Richardson, G.P. (2003). A receptor-like inositol lipid phosphatase is required for the maturation of developing cochlear hair bundles. J. Neurosci. *23*, 9208–9219.
22. Self, T., Sobe, T., Copeland, N.G., Jenkins, N.A., Avraham, K.B., and Steel, K.P. (1999). Role of myosin VI in the differentiation of cochlear hair cells. Dev. Biol. *214*, 331–341.
23. Marsick, B.M., San Miguel-Ruiz, J.E., and Letourneau, P.C. (2012). Activation of Ezrin/Radixin/Moesin Mediates Attractive Growth Cone Guidance through Regulation of Growth Cone Actin and Adhesion Receptors. J. Neurosci. *32*, 282–296.
24. Pataky, F., Pironkova, R., and Hudspeth, A.J. (2004). Radixin is a constituent of stereocilia in hair cells. Proc. Natl. Acad. Sci. USA *101*, 2601–2606.

25. Kitajiri, S.i., Fukumoto, K., Hata, M., Sasaki, H., Katsuno, T., Nakagawa, T., Ito, J., Tsukita, S., and Tsukita, S. (2004). Radixin deficiency causes deafness associated with progressive degeneration of cochlear stereocilia. J. Cell Biol. *166*, 559–570.

26. Prasad, S., Vona, B., Diñeiro, M., Costales, M., González-Aguado, R., Fontalba, A., Diego-Pérez, C., Subasioglu, A., Bademci, G., Tekin, M., et al. (2020). Radixin modulates the function of outer hair cell stereocilia. Commun. Biol. *3*, 792.

27. Rehman, A.U., Morell, R.J., Belyantseva, I.A., Khan, S.Y., Boger, E.T., Shahzad, M., Ahmed, Z.M., Riazuddin, S., Khan, S.N., Riazuddin, S., and Friedman, T.B. (2010). Targeted Capture and Next-Generation Sequencing Identifies C9orf75, Encoding Taperin, as the Mutated Gene in Nonsyndromic Deafness DFNB79. Am. J. Hum. Genet. *86*, 378–388.

28. Huang, B., Babcock, H., and Zhuang, X. (2010). Breaking the diffraction barrier: super-resolution imaging of cells. Cell *143*, 1047–1058.

29. Harke, B., Keller, J., Ullal, C.K., Westphal, V., Schönle, A., and Hell, S.W. (2008). Resolution scaling in STED microscopy. Opt. Express *16*, 4154–4162.

30. Liu, Y., Qi, J., Chen, X., Tang, M., Chu, C., Zhu, W., Li, H., Tian, C., Yang, G., Zhong, C., et al. (2019). Critical role of spectrin in hearing development and deafness. Sci. Adv. *5*, eaav7803.

31. Zhao, B., Wu, Z., and Müller, U. (2016). Murine Fam65b forms ring-like structures at the base of stereocilia critical for mechanosensory hair cell function. Elife *5*, e14222.

32. She, K., Liu, Y., Zhao, Q., Jin, X., Yang, Y., Su, J., Li, R., Song, L., Xiao, J., Yao, S., et al. (2023). Dual-AAV split prime editor corrects the mutation and phenotype in mice with inherited retinal degeneration. Signal Transduct. Target. Ther. *8*, 57.

33. Landegger, L.D., Pan, B., Askew, C., Wassmer, S.J., Gluck, S.D., Galvin, A., Taylor, R., Forge, A., Stankovic, K.M., Holt, J.R., and Vandenberghe, L.H. (2017). A synthetic AAV vector enables safe and efficient gene transfer to the mammalian inner ear. Nat. Biotechnol. *35*, 280–284.

34. Perrin, B.J., Sonnemann, K.J., and Ervasti, J.M. (2010). beta-actin and gamma-actin are each dispensable for auditory hair cell development but required for Stereocilia maintenance. Plos Genet. *6*, e1001158.

35. Salles, F.T., Andrade, L.R., Tanda, S., Grati, M., Plona, K.L., Gagnon, L.H., Johnson, K.R., Kachar, B., and Berryman, M.A. (2014). CLIC5 stabilizes membrane-actin filament linkages at the base of hair cell stereocilia in a molecular complex with radixin, taperin, and myosin VI. Cytoskeleton *71*, 61–78.

36. Goodyear, R., and Richardson, G. (1992). Distribution of the 275 kD hair cell antigen and cell surface specialisations on auditory and vestibular hair bundles in the chicken inner ear. J. Comp. Neurol. *325*, 243–256.

37. Sakaguchi, H., Tokita, J., Naoz, M., Bowen-Pope, D., Gov, N.S., and Kachar, B. (2008). Dynamic compartmentalization of protein tyrosine phosphatase receptor Q at the proximal end of stereocilia: implication of myosin VI-based transport. Cell Motil. Cytoskeleton *65*, 528–538.

38. Bindels, D.S., Haarbosch, L., van Weeren, L., Postma, M., Wiese, K.E., Mastop, M., Aumonier, S., Gotthard, G., Royant, A., Hink, M.A., and Gadella, T.W.J., Jr. (2017). mScarlet: a bright monomeric red fluorescent protein for cellular imaging. Nat. Methods *14*, 53–56.

39. Yen, L., Svendsen, J., Lee, J.S., Gray, J.T., Magnier, M., Baba, T., D'Amato, R.J., and Mulligan, R.C. (2004). Exogenous control of mammalian gene expression through modulation of RNA self-cleavage. Nature *431*, 471–476.

40. Zhong, G., Wang, H., He, W., Li, Y., Mou, H., Tickner, Z.J., Tran, M.H., Ou, T., Yin, Y., Diao, H., and Farzan, M. (2020). A reversible RNA on-switch that controls gene expression of AAV-delivered therapeutics in vivo. Nat. Biotechnol. *38*, 169–175.

41. Vidović, D., Carlon, M.S., da Cunha, M.F., Dekkers, J.F., Hollenhorst, M.I., Bijvelds, M.J.C., Ramalho, A.S., Van den Haute, C., Ferrante, M., Baekelandt, V., et al. (2016). rAAV-CFTRDeltaR Rescues the Cystic Fibrosis Phenotype in Human Intestinal Organoids and Cystic Fibrosis Mice. Am. J. Respir. Crit. Care Med. *193*, 288–298.

42. Ostedgaard, L.S., Rokhlina, T., Karp, P.H., Lashmit, P., Afione, S., Schmidt, M., Zabner, J., Stinski, M.F., Chiorini, J.A., and Welsh, M.J. (2005). A shortened adeno-associated virus expression cassette for CFTR gene transfer to cystic fibrosis airway epithelia. Proc. Natl. Acad. Sci. USA *102*, 2952–2957.

43. Qi, J., Liu, Y., Chu, C., Chen, X., Zhu, W., Shu, Y., He, S., Chai, R., and Zhong, G. (2019). A cytoskeleton structure revealed by super-resolution fluorescence imaging in inner ear hair cells. Cell Discov. *5*, 12.

44. Xu, K., Zhong, G., and Zhuang, X. (2013). Actin, spectrin, and associated proteins form a periodic cytoskeletal structure in axons. Science *339*, 452–456.

45. Fettiplace, R., and Kim, K.X. (2014). The physiology of mechanoelectrical transduction channels in hearing. Physiol. Rev. *94*, 951–986.

46. Zhao, B., and Müller, U. (2015). The elusive mechanotransduction machinery of hair cells. Curr. Opin. Neurobiol. *34*, 172–179.

47. Zhao, X., Jin, C., Dong, T., Sun, Z., Zheng, X., Feng, B., Cheng, Z., Li, X., Tao, Y., and Wu, H. (2020). Characterization of promoters for adeno-associated virus mediated efficient Cas9 activation in adult Cas9 knock-in murine cochleae. Hear. Res. *394*, 107999.

48. Balducci, C., Mancini, S., Minniti, S., La Vitola, P., Zotti, M., Sancini, G., Mauri, M., Cagnotto, A., Colombo, L., Fiordaliso, F., et al. (2014). Multifunctional liposomes reduce brain beta-amyloid burden and ameliorate memory impairment in Alzheimer's disease mouse models. J. Neurosci. *34*, 14022–14031.

49. Tan, F., Chu, C., Qi, J., Li, W., You, D., Li, K., Chen, X., Zhao, W., Cheng, C., Liu, X., et al. (2019). AAV-ie enables safe and efficient gene transfer to inner ear cells. Nat. Commun. *10*, 3733.

50. Chen, Y.H., Keiser, M.S., and Davidson, B.L. (2018). Adeno-Associated Virus Production, Purification, and Titering. Curr. Protoc. Mouse Biol. *8*, e56.

51. Gao, G., Qu, G., Burnham, M.S., Huang, J., Chirmule, N., Joshi, B., Yu, Q.C., Marsh, J.A., Conceicao, C.M., and Wilson, J.M. (2000). Purification of recombinant adeno-associated virus vectors by column chromatography and its performance in vivo. Hum. Gene Ther. *11*, 2079–2091.